IOP Publishing Journal of Micromechanics and Microengineering
J. Micromech. Microeng. **26** (2016) 037001 (5pp) doi:10.1088/0960-1317/26/3/037001

Technical Note

Nanopore fabrication in silicon oxynitride membranes by heating Au-particles

L J de Vreede, M Schmidt Muniz, A van den Berg and J C T Eijkel

BIOS lab-on-a-chip group, MESA + Institute for Nanotechnology, MIRA Institute for Biomedical Technology and Technical Medicine, University of Twente, The Netherlands

E-mail: l.j.devreede@utwente.nl

Received 9 November 2015, revised 23 December 2015
Accepted for publication 4 January 2016
Published 8 February 2016

Abstract

We report the fabrication of nanopores in a silicon oxynitride (SiON) membrane by heating a silicon rich-silicon nitride (SiRN) membrane with a gold nanoparticle array deposited on its surface. The gold nanoparticle array was realized by photolithography and the membrane by wet-etching. The entire process is wafer scale. Nanopore through-holes of an average diameter of 150 nm were produced in a ~22 nm thick membrane. Membranes and nanopores were characterized by atomic force microscopy, scanning transmission electron microscopy, and x-ray photo-electron spectrocopy.

Keywords: nanopore, gold, dewetting, SiRN oxidation, SiON

S Online supplementary data available from stacks.iop.org/JMM/26/037001/mmedia

(Some figures may appear in colour only in the online journal)

1. Introduction

Nanopores in thin membranes are of great interest for biosensing and separation processes with applications in sieving [1], molecular separation [2], DNA analysis [3], and DNA sequencing [4]. The creation of nanopores for such applications typically relies on a combination of a membrane fabrication method with an established nanopore formation technology like focused ion beam milling [5, 6], track etching [7], electron beam writing [8], or dielectric breakdown [9]. Another method is to use dry etching processes combined with Au particles, where the etch rate is locally enhanced around the Au particle creating a nanopore [10]. In a recent paper we showed the fabrication of dead-end nanopores in SiO_2 by a novel technique based on gold nanoparticle penetration in fused silica upon heating, as well as the preliminary results of the manufacturing of through-holes in a SiO_2 membrane [11]. Here we demonstrate a manufacturing process on the basis of this new technique that results in nanopore through-holes in membranes of SiON.

2. Materials and methods

To create the membrane with nanopores, low-stress (50 MPa) SiRN with a thickness of 36 nm was grown on p-type (1 0 0) one-side polished silicon wafers. Olin 906–12 photoresist was applied by spin coating at 6000 rpm, creating a 1 μm thick photoresist layer. The photoresist layer was exposed with a dose of 12 mW s^{-1} using a mask containing 2 μm circular features that were 5 μm spaced. After photoresist development and an ozone treatment to remove any residual photoresist from the nitride layer, gold with a thickness of 20 nm was sputtered. A lift off was done in acetone for 15 min. The substrate with the nitride and gold pattern was then again spin-coated with a photoresist layer, Olin 907–17 at 4000 rpm, and after photolithography the chromium layer with a thickness of 40 nm was sputtered over the silicon nitride and gold pattern.

 © 2016 IOP Publishing Ltd Printed in the UK

Photolithography was then performed on the non-polished backside of the wafer. The SiRN layer on the backside of the wafer then functioned as a potassium hydroxide (KOH) etch mask. The backside SiRN layer was plasma etched for 90 s (gas flow 25 sccm CHF_3, 5 sccm O_2, pressure 10 mTorr, power 60 W). The wafers were etched up to the topside SiRN membrane using KOH 25% at 75 °C for 8 h. The chromium layer was removed with chromium etchant (Chrome etch n° 1, MicroChemicals GmbH). The wafer was then cleaved in 16 mm square chips. To create nanopore through-holes in the SiRN membranes, the chips were then placed in a furnace for a heat treatment for 6 h. The furnace heated the samples to 1067 °C ± 5 °C.

2.1. Characterization

The properties of the thin film before and after heat treatment were investigated using x-ray photo-electron spectrocopy (XPS) and a series of etching experiments combined with ellipsometry. The etching was performed in steps of one minute for a total of 10 min in KOH 25%, 75 °C. After each minute of etching the layer thickness and refractive index were measured by ellipsometry using a J. A. Woollam ellipsometer. After 10 min of etching, three etch time intervals of 5 min were applied. The nanopores were inspected using scanning transmission electron microscopy.

3. Results and discussion

3.1. Nanopores

In our previous research concerning Au penetration in SiO_2, we found that the heat treatment initially caused dewetting of the gold patches to form gold nanoparticles. This dewetting was followed by the particles penetrating the SiO_2 layer and forming dead-end nanopores in the bulk material. We proposed a mechanism based on a combination of gold evaporation coupled to continuous SiO_2 transport to the Au/SiO_2/air triple line driven by capillary forces, forming the pores [11]. In our present research, as in the case of SiO_2, we found that nanopores had formed in the membranes. The membranes also oxidized from SiRN into SiON during the heat treatment, which was performed in ambient air. The proposed pore formation mechanism is shown in the schematic diagram in figure 1. In general, the surface energy of the materials involved provides a specific air phase angle (θ_A) when a droplet of gold is placed on a ceramic surface [11, 12]. When the initial shape of the gold nanoparticle does not provide the desired angle between Au and the ceramic, ceramic material diffuses toward the Au/ceramic/air triple line to reach equilibrium, forming a ridge at the particle diameter. When gold continuously evaporates, this process proceeds over a long time, whereby the ceramic material is continuously transported from below the gold to the triple line, leading to pore formation (see figure 1). When the ceramic material is a thin membrane, a through-hole is formed, as evidenced by the scanning transmission electron microscopy (STEM) pictures of figures 2(b) and (c).

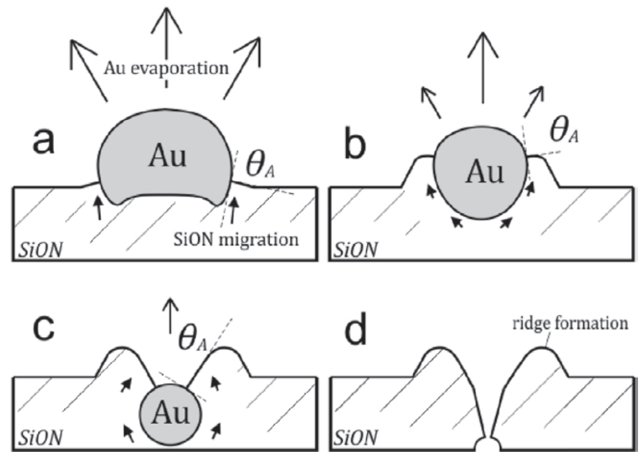

Figure 1. Schematic representation of the proposed nanopore through-hole formation mechanism. SiON migration to the triple line to maintain the angle θ_A between the gold and the SiON combined with the continuous evaporation of gold creates the nanopores (modified with permission from [11], copyright 2015 American Chemical Society).

Membranes of 80 by 80 μm square with 256 patches of gold, after the heat treatment contained 256 nanopores with a spacing of 5 μm. To determine the size of the pores, STEM pictures of thirty holes were measured using ImageJ software. It was found that the shape was approximately circular with an area-averaged diameter of 167 nm and a standard deviation of 48 nm. Details of the size distribution are given in the supplementary information (stacks.iop.org/JMM/26/037001/mmedia). The pores were always located inside the perimeter of the original deposited Au patch.

3.2. Membrane oxidation and buckling

Figure 2(a) also shows that the (initially flat) membranes became buckled in the process. Membrane buckling on these scales is a result of internal material stresses [13]. A possible explanation is an oxidation of the SiRN layer, which will cause a volume increase. This oxidation is expected since the heat treatment took place in an ambient atmosphere. The oxidation of SiRN increases the membrane thickness and results in a layered configuration of SiO_2, SiON, and SiRN [14]. Another possible cause of the membrane buckling is the oxidation of the bare silicon on which the membrane is suspended after KOH etching. Finally, although expected to make only a minor contribution, the creation of the nanopore through-holes can also have an effect on the buckling since it decreases the membrane stiffness [15]. To assess the oxidation state of the SiRN, the layer thickness and refractive index were measured by ellipsometry on the Si at a location adjacent to the membrane. Measurements before and after heat treatment showed that the layer thickness increased from 36 nm before to 42 nm after heat treatment. The layering of the oxidized SiRN layer was investigated in two ways. One method was by means of XPS, and the other method was by KOH etching at given time intervals followed by ellipsometry measurements of the layer. The graphs in figures 3(a) and (b) show the XPS measurements of the layer before and after the

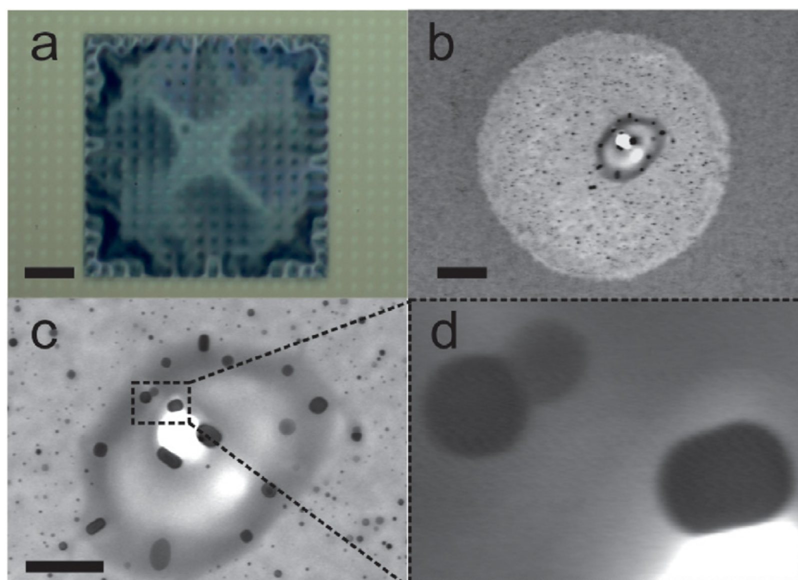

Figure 2. (a) Overview of a SiON membrane with a nanopore through-hole array. The scale bar represents 20 μm. The membrane can be seen to be buckled. In (b) a single nanopore is shown, the scale bar represents 400 nm. (c) Shows the nanopore through-hole, with in detail crystallites thought to be of Au and Au-Si, the scale bar represents 200 nm. (d) Is a close-up of the three crystallites.

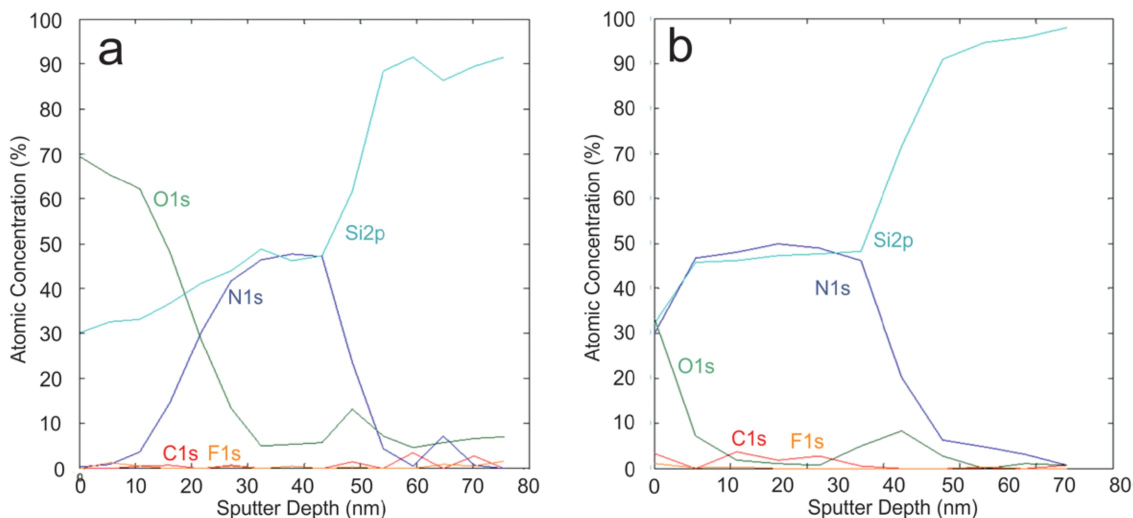

Figure 3. (a) The elemental content depth profile of the oxidized SiRN layer on the Si substrate before KOH etching. The atomic concentration is given for carbon (C1s), nitrogen (N1s), oxygen (O1s), fluor (F1s), and silicon (Si2p). Before sputtering the O1s content is 70% and the Si2p content 30%. On increasing the sputter depth the ratio of the oxygen and nitrogen content changes, indicating the presence of a gradient of SiON ending at a depth of 27 nm and followed by a layer of SiN. At a 45 nm sputter depth Si remained (Si2p). (b) Shows the atomic concentrations after KOH etching, removing the SiO_2 and leaving SiON and SiN on Si.

etching experiment. Figure 3(a) shows the layer before etching and reveals that the surface layer has a 70% oxygen content and a 30% silicon content (SiO_2). The subsequent gradual decline in oxygen content and the increase in nitrogen content in the depth profile is evidence of a SiON layer. At a sputter depth of 30 nm the oxygen is removed and a SiN layer remains (approximately 50% nitrogen and 50% silicon). Figure 3(b) shows the XPS data of the surface after KOH etching. A ratio of 33% oxygen, 33% silicon, and 30% nitrogen is observed (and 4% fluor and carbon content), indicating the presence of SiON.

Figure 4 shows the measured layer thickness after the subsequent etch steps. Two stages can be clearly distinguished. The first stage from 0 to 10 min shows an etching rate of 1.4 nm min^{-1}, in which a 16 nm layer is etched away. The second stage, from minute 10 to minute 25 shows a much slower etch rate of 0.06 nm min^{-1} [16]. The ellipsometry data of the layer after 25 min of etching show a refractive index of 2.06 of the remaining 25 nm thick layer. This value is in good agreement with the refractive index of SiRN, which ranges from 1.99 to 2.35 [17, 18]. The etch rate of the second stage in KOH 25%, 75 °C is 0.06 nm min^{-1}. These data compare well with the XPS data in figures 3(a) and (b), which shows a stacked layer of SiO_2, SiON, SiN, and Si with a total thickness of 44 nm (at a 44 nm sputter depth a strong increase in Si content is shown). From the sputter depth profile we then concluded that the SiO_2 layer thickness is 16 nm, the SiON layer thickness is 11 nm, and the SiRN layer is 17 nm. As is shown, more than half of the initial 44 nm thickness has thus

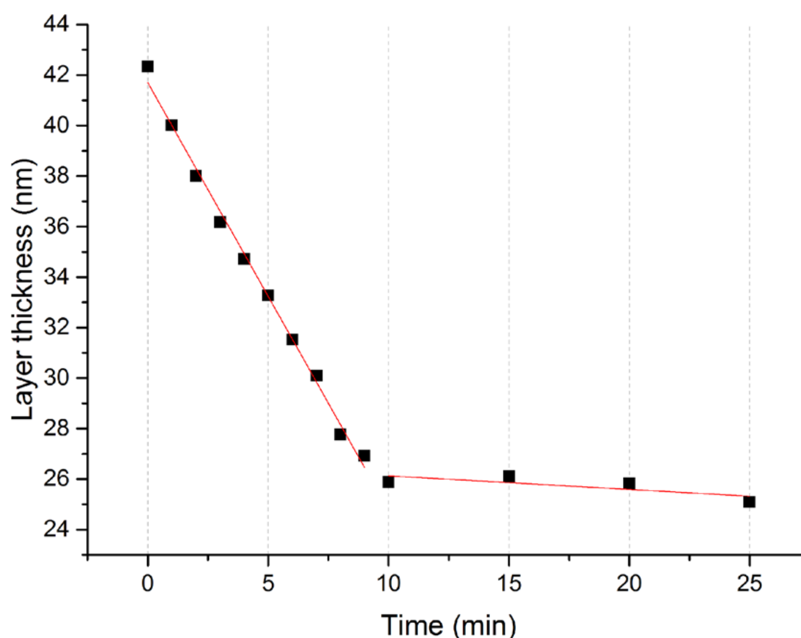

Figure 4. The thickness of the oxidized layer on top of the silicon adjacent to the membrane after subsequent KOH etch steps of the indicated time, for three experiments. Linear fits to the data for the period before and after 10 min are shown. The decrease in layer thickness in the first 10 etch steps of 16 nm is the etching of the SiO_2 layer.

converted into either SiO_2 or SiON. Since the oxidation of the membrane proceeded from two sides, we expect that the initial SiRN membrane has fully transformed into SiON. It is thus not surprising that the buckling induced by the heat treatment was still present after KOH etching.

3.3. Nanopore formation mechanism

In STEM imaging a darker shade indicates either a denser material or a thicker layer [19]. On the other hand, when no material is present, the image appears white since electrons can then travel directly from the source to the detector. The STEM image of figure 2(b) shows that a circular area with a diameter of 2 μm (the original dimension of the deposited Au patch) has a lighter shade compared to the rest of the membrane. The 2 μm diameter area also has a high density of small crystalline shapes, while the direct area around the pore shows just a few larger crystals. Atomic force microscopy (AFM) measurements of the former Au patch area show that it lies about 5 nm deeper than the remainder of the membrane (see supplementary information (stacks.iop.org/JMM/26/037001/mmedia)). In figure 2(c) darker and lighter crystalline shapes can be distinguished close to the pore, as is clearly visible in the enlarged area in figure 2(d).

Our hypothesis is that the crystalline shapes in the 2 μm diameter area are crystallites of Au or Si, or of Au-Si alloys. The Au crystallites could have formed due to break up of the Au patch, when it would show a pinch-off instead of fully dewetting into a singular particle. Also, Si clustering during heat treatment can take place within SiRN layers [18]. Subsequent reactions between the Au and Si clusters from the SiRN membrane material have not been ruled out [20]. Alloy formation between Au and Si is known to occur at higher temperatures [21]. The molar ratio of Si and N in a SiRN layer is 1.04, implying an excess of Si with respect to Si_3N_4 [17], which could have alloyed with the Au.

Since oxidation plays an important role in this process, the lighter shaded circular area with dark crystals in the SiON surface at the original location of the patterned gold could be explained by oxidation of the initial SiRN layer. The 20 nm gold layer is likely to break up at around 400 °C [22]. Oxidation of the SiRN layer could have appeared during the ramp-up time of the furnace reaching the temperature at which dewetting of Au takes place. Within the circular area a darker ring around the nanopore can be observed, as shown in figure 2(c). This ring is a ridge, as mentioned in the discussion concerning figure 1, and is shown in an AFM picture in the supplementary information. This ridge formation occurs before pore formation, as was explained in our previous paper on Au nanopore formation in SiO_2. After etching in 1%HF for 20 min the ridge disappeared (see supplementary information), while the rest of the 2 μm diameter area remained, indicating a ridge with a high SiO_2 content. At the perimeter of the ridge large dark crystals can be seen and also at the perimeter of the pore large dark crystals are present. We expect here crystals could have grown larger because the surface was for a longer time in contact with the Au particle, which retreated slowly after ridging started.

4. Conclusion

The method described here proves to be capable of creating nanopore through-holes in a ~20 nm thick SiON membrane. By starting the process with a 36 nm thick SiRN membrane with Au patches on top, a heat treatment by a combination of oxidation, capillary action, and gold evaporation leads to wafer scalable nanopore through-hole formation. XPS

measurements show oxidation of the original SiRN into SiON. Buckling of the membrane is also observed, which is a result of the consequent volume increase. We show a proof of principle of a new method for nanopore through-hole fabrication, potentially competing with methods like electron beam writing or ion beam milling.

Acknowledgments

This work is supported by NanoNextNL, a micro and nanotechnology consortium of the Government of the Netherlands and 130 partners.

References

[1] Choi D H, Han Y D, Lee B K, Choi S J, Yoon H C, Lee D S and Yoon J B 2012 Nanosieves: use of a columnar metal thin film as a nanosieve with sub-10 nm pores *Adv. Mater.* **24** 4408–13

[2] Montagne F, Blondiaux N, Bokjo A and Pugin R 2012 Molecular transport through nanoporous silicon nitride membranes produced from sefl-assembling block copolymers *Nanoscale* **4** 5880–6

[3] Li J, Gershow M, Stein D, Brandin E and Golovchenko J A 2003 DNA molecules and configurations in a solid-state nanopore microscope *Nat. Mater.* **2** 611–5

[4] Dekker C 2007 Solid-state nanopores *Nat. Nanotechnol* **2** 209–15

[5] Tong H D, Jansen H V, Gadgil V J, Bostan C G, Berenschot E, van Rijn C J M and Elwenspoek M 2004 Silicon nitride nanosieve membrane *Nano Lett.* **4** 283–7

[6] Li C, Zhao L, Mao Y, Wu W and Xu J 2015 Focus-ion-beam induced rayleigh-plateau instability for diversiform suspended nanostructure fabrication *Sci. Rep.* **5** 8236

[7] Vlassiouk I, Apel P Y, Dmitriev S N, Healy K and Siwy Z S 2009 Versatile ultrathin nanoporous silicon nitride membranes *PNAS* **106** 21039–44

[8] Storm A J, Chen J H, Ling X S, Zandbergen H W and Dekker C 2003 Fabrication of solid-state nanopores with single-nanometre precision *Nat. Mater.* **2** 537–40

[9] Kwok H, Briggs K, Tabard-Cossa V 2014 Nanopore fabrication by controlled dielectric breakdown *PLoS ONE* **9** e92880

[10] James T, Kalinin Y V, Chan C, Randhawa J S, Gaevski M and Gracias D H 2012 Voltage-gated ion transport through semiconducting conical nanopores formed by metal nanoparticle-assisted plasma etching *Nano Lett.* **12** 3437–42

[11] de Vreede L J, van den Berg A and Eijkel J C T 2015 Nanopore fabrication by heating Au particles on ceramic substrates *Nano Lett.* **15** 727–31

[12] Smith C 1948 Grains, phases and interfaces—an interpretation of microstructure *Trans. Metall. Soc. AIME* **175** 15–51

[13] Ziebart V, Paul O and Baltes H 1999 Strongly buckled square micromachined membranes *J. Microelectromech. Syst.* **8** 423–32

[14] Raider S I, Flitsch R, Aboaf J A and Pliskin W A 1976 Surface oxidation of Si_3N_4 films *J. Electrochem. Soc.* **123** 560–5

[15] Kuiper S, Brink R, Nijdam W, Krijnen G J M and Elwenspoek M C 2002 Ceramic microsieves: influence of perforation shape and distribution on flow resistance and membrane strength *J. Membr. Sci.* **196** 149–57

[16] Sheldon B W 1996 Silicon Nitride oxidation based on oxynitride interlayers with graded stoichiometry *J. Am. Ceram. Soc.* **79** 2993–6

[17] Gardeniers J G E, Tilmans H A C and Visser C C G 1996 LPCVD silicon-rich silicon nitride films for applications in micromechanics, studied with statistical expermental design *J. Vac. Sci. Technol.* A **14** 2879–92

[18] Andersen K N, Svendsen W E, Stimpel-Lindner T, Sulima T and Bäumgartner H 2005 Annealing and deposition effects of the chemical composition of silicon-rich nitride *App. Surf. Sci.* **243** 401–8

[19] Rath A, Dash J K, Juluri R R, Rosenauer A and Satyam P V 2011 Temperature-dependent electron microscopy study of Au thin films on Si (1 0 0) with and without native oxide layer as barrier at the interface *J. Phys. D: Appl. Phys.* **44** 115301

[20] Chakraborty S, Kamila J, Rout B, Satpati B, Satyam P V, Sundaravel B and Dev B N 2004 Shape variation in epitaxial microstructures of gold silicide grown on Br-passivated Si(1 1 1) surfaces *Surf. Sci.* **549** 149–56

[21] Okamoto H, Massalski T B 1983 The Au-Si (Gold-Silicon) system *Bull. Alloy Phase Diagrams* **4** 190–8

[22] Mueller C M, Spolenak R 2013 Dewetting of Au and AuPt alloy films: a dewetting zone model *J. Appl. Phys.* **113** 094301